Numerical simulations of the evolution of Taylor cells from a growing boundary layer on the inner cylinder of a high radius ratio Taylor-Couette system

W. M. J. Batten, N. W. Bressloff, and S. R. Turnock
School of Engineering Sciences, University of Southampton, Highfield, Southampton SO17 3BJ, United Kingdom
(Received 25 March 2002; published 9 December 2002)

The Taylor-Couette flow in the gap between two concentric cylinders has been studied numerically to show the evolution of Taylor vortices from pairs of ring-shaped vortices, at Reynolds numbers of 5×10^3 and 8×10^3 based upon the gap width. The cylinders have a high radius ratio of 0.985 and the inner cylinder rotates within a stationary outer cylinder. Initially, ring-shaped vortices are generated at the surface of the inner cylinder and spread into the gap. This is distinctly different from the formation of laminar Taylor vortices that grow from the end walls. Mixing of these ring-shaped vortices with the developing Couette flow then occurs and further ring-shaped vortices are generated. Some of these dominate the flow and begin to form Taylor vortices. Finally the Taylor vortices are stabilized and further vortex formation ceases. An analysis is also presented of the variation of shear stress with time.

DOI: 10.1103/PhysRevE.66.066302 PACS number(s): 47.54.+r, 47.27.−i, 83.85.Pt

I. INTRODUCTION

The Taylor-Couette flow in the gap between a rotating inner cylinder and a fixed outer cylinder is of interest in several engineering applications, such as motors, filters, pumps, and journal bearings. The motivation for this work stemmed from the development of a novel underwater-integrated electrical thruster unit [1,2]. A significant source of power loss in the electrical thruster arises from the frictional resistance that occurs between two such cylinders. The transient development of the Taylor-Couette flow is of particular interest since it effects the number of Taylor cells and hence the friction loss; the latter being dependent upon the length of the vortices [3,4].

This paper presents an insight into the evolution of Taylor vortices in the gap between a stationary outer cylinder and an inner cylinder rotated from rest. Of particular interest in the current context is the fact that, initially, pairs of ring-shaped vortices appear to emerge from the boundary layer on the inner cylinder. These vortices may exhibit flow behavior similar to Görtler-type instabilities. Although Görtler's original work applied to concave surfaces [5], there is other evidence suggesting that the boundary layers on either cylinder wall may be subject to similar instabilities [6–8].

The Taylor-Couette flow has been studied since Taylor [9] reported the formation of an array of alternating laminar toroidal vortices at a particular speed, dependent upon the geometry of the problem. The Taylor number is defined as

$$\mathrm{Ta}=\frac{\mathrm{Re}^2 d}{R_1}, \tag{1}$$

where Re is the Reynolds number,

$$\mathrm{Re}=\frac{U_1 d}{\nu}, \tag{2}$$

and d is the gap width, R_1 is the inner radius, U_1 is the speed of the inner cylinder, and ν is the kinematic viscosity. The Taylor number at which these vortices first appear is known as the critical Taylor number, Ta_c. Initially, laminar Taylor vortices form at the end walls, then Taylor vortices form adjacent to the end wall vortex and the vortex pattern develops inwards. This pattern then completes in the center and the cell lengths adjust if required [10].

Above Ta_c, the flow undergoes a series of bifurcations from axially stable Taylor vortices through various wavy states until the flow becomes chaotic. Koschmieder [11] stated that when $\mathrm{Ta}\approx 1000\mathrm{Ta}_c$, order emerges from chaotic flow and the flow is turbulent with axisymmetric stable uniform vortices. As the Taylor number increases, the flow undergoes a transition from, "soft" turbulence to "hard" turbulence [3,12]. In the "soft" turbulence, turbulent production is dominated by the interaction between vortices, while the "hard" turbulence is dominated by turbulent production associated with the walls [13]. Koschmieder showed that the turbulent Taylor vortex cell length is highly dependent upon the start-up conditions. The vortex length varied from 20% larger than the critical value, during rapid accelerations to 70% larger during quasisteady accelerations [14].

Barcilon *et al.* [6] showed the formation of "herring-bone"-like streaks in photographs of, turbulent Taylor vortices. They suggested that these patterns were due to the existence of Görtler vortices forming on the outer cylinder. Subsequent visualization studies at a different radius ratio have, however, not shown the formation of similar "herring bone" patterns present in kaleidoscope visualization, for example, see Refs. [3,14].

Wei *et al.* [8] also claim to have observed Görtler-like vortices for a range of Taylor numbers and for three radius ratios [$\eta=$ 0.084, 0.5, and 0.88, where $\eta=R_1/(R_1+d)$] forming on the inner cylinder. These vortices were observed using laser-induced fluorescence (LIF) for all three radius ratios and the study established that the vortex patterns were not due to the injection of the dye. Visualization using $\eta=0.5$ demonstrated the transport of these vortices along the length of the inner cylinder from the vortex inflow boundary. Results obtained using a large gap, $\eta=0.084$, also showed stronger vortices than those associated with the Taylor vor-

tices. For the high radius ratio, $\eta=0.88$, the so-called Görtler-like vortices were also observed, but for high speeds no images from the LIF were presented, due to problems of image reproduction. Instead aluminuma particle photographs were shown and these are suggestive of "herring-bone" patterns similar to Barcilon *et al.* [6]

II. NUMERICAL METHOD

In order to study the development of Taylor cells from vortex disturbances on the inner cylinder, a full three-dimensional (3D) direct numerical simulation (DNS) is required, since, even in flows where the mean velocities and pressures vary in one or two dimensions, turbulent fluctuations always have a three-dimensional spatial character. To perform a full 3D simulation that resolves all the eddies was beyond our available computing resources at the present time. So, for this initial phase of research, the gap was modeled as a 2D slice between a pair of periodic boundaries in the azimuthal direction. This type of solution is akin to a 1D DNS solution of plane Couette flow. The authors realize that this is an artificial approach to DNS since only in 3D is it possible to resolve the turbulent eddies, but the analysis provides a useful insight into the formation of turbulent Taylor vortices at an affordable computational cost.

An in-house parallel finite volume code was used with the pressure implicit splitting of operators algorithm [15] to solve the incompressible Navier-Stokes equations

$$\frac{\partial u_i}{\partial t}+u_j\frac{\partial u_i}{\partial x_j}=-\frac{1}{\rho}\frac{\partial p}{\partial x_i}+\nu\frac{\partial^2 u_i}{\partial x_j\partial x_j} \tag{3}$$

and

$$\frac{\partial u_i}{\partial x_i}=0, \tag{4}$$

where u is the velocity and p denotes pressure, x is the spatial coordinate, the subscripts i and j symbolize coordinate direction in the field and ρ is the fluid density. For the purpose of this limited study only second-order accuracy was used in both space and time. A no-slip boundary condition was applied to all walls. The rotating walls were accelerated linearly and the fluid was initially at rest.

A number of investigative calculations were performed in preparation for the final simulations. All simulations were based upon the thruster unit, $\eta=0.985$, $R_1=0.128$ m, and $\nu=1\times10^{-6}\ m^2/s$. Initially, simulations were carried out on a much smaller domain; but it was discovered that at the block interfaces, vortices were forming at the inner cylinder. To establish that the effect of the block interface was not the sole cause of vortices, the domain was extended to half the length of that in the thruster, $\Gamma=d/L=16$, where L is the length of the gap and a single block interface is in the middle. To determine the effect of end boundaries, one end boundary was rotating while the other was stationary. To demonstrate the effect of speed, tests were carried out at two Re of 5×10^3 and 8×10^3.

In order to ensure that sufficient cells were placed across the gap to accurately model the flow, 150 cells were used. This is more than twice that used for the turbulence modeling in Ref. [13]. The grid was uniformly expanding and then contracting across the gap. The first node was placed well inside the laminar sublayer. For $\mathrm{Re}=5\times10^3$, the first node was at $n^+=(n\sqrt{\tau_w/\rho})/\nu=0.3$, where n is the distance from a cylinder wall, τ_w is the shear stress at a cylinder. We used

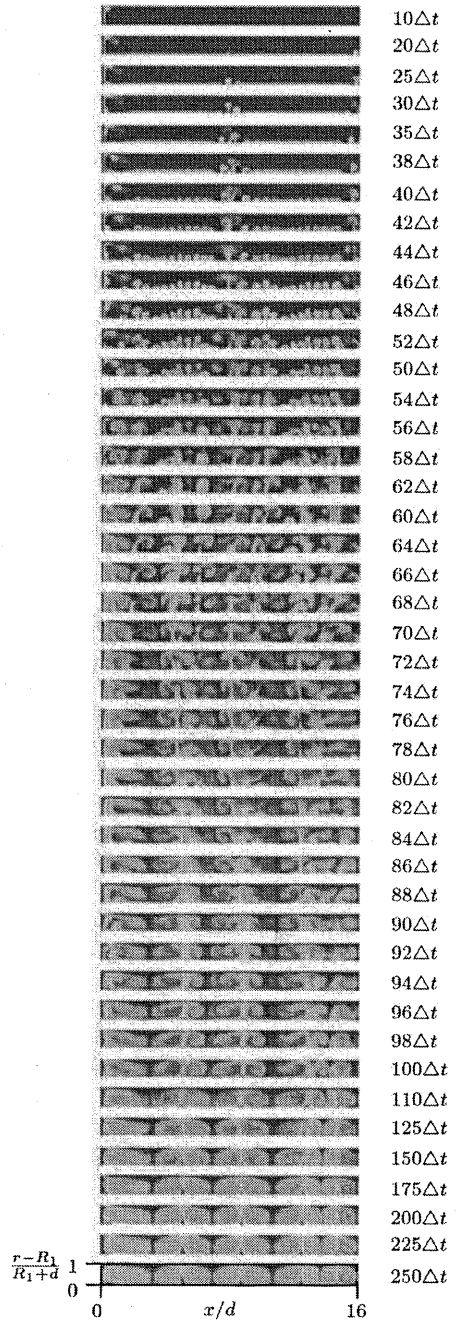

FIG. 1. The evolution of stable Taylor vortices, at $\mathrm{Re}=5\times10^3$.

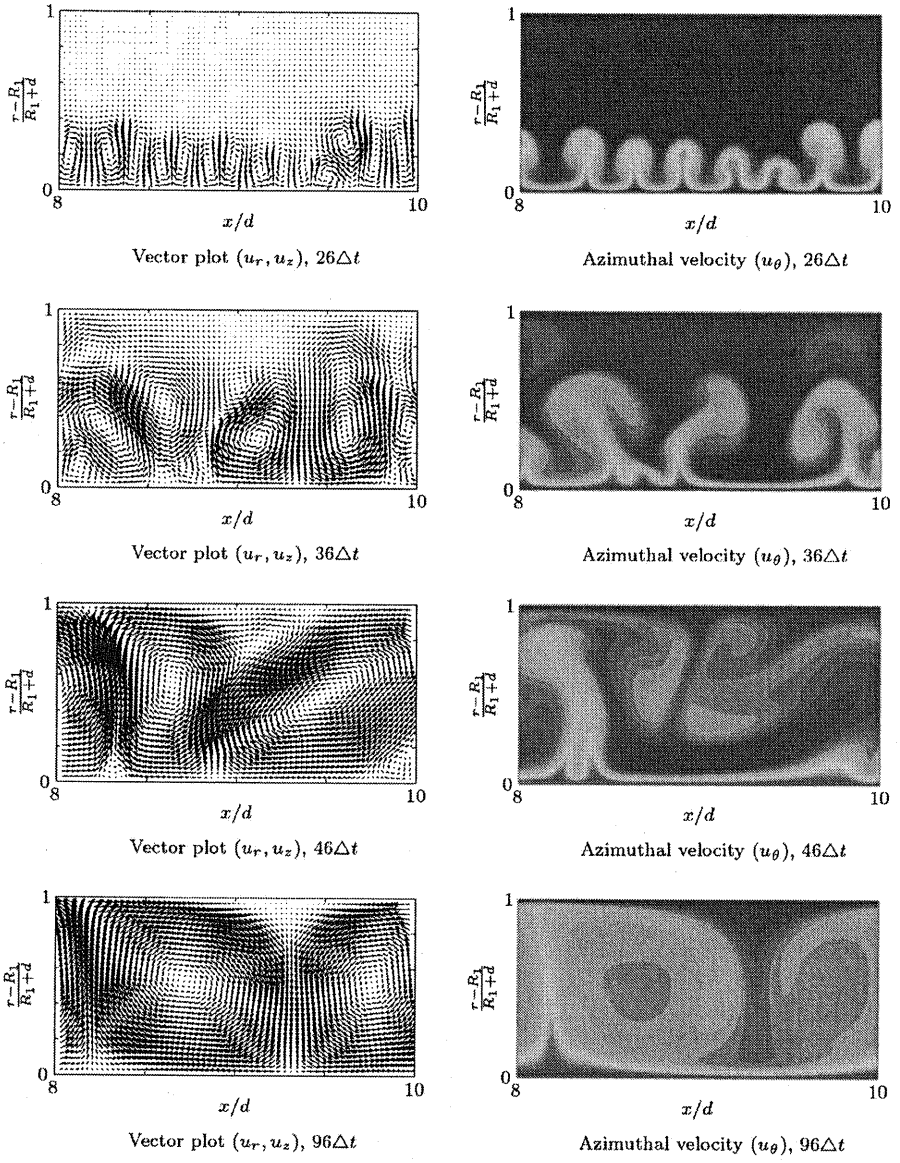

FIG. 2. Series of close-up images showing the formation of one Taylor vortex from several of initial pairs of ring-shaped vortices, at $\mathrm{Re}=8\times10^3$.

1000 cells along the length producing uniform cells in the center of the domain.

A time step of 10^{-5} s was used and the simulation run for 1.5 s. A complete set of data was stored every 250 time steps, giving a time interval, $\Delta t=0.0025$ s. The complete calculation required 8 days on 6 PIII 500 MHz processors.

III. RESULTS AND DISCUSSION

Figure 1 represents the development of Taylor vortices as a series of azimuthal velocity plots for $\mathrm{Re}=5\times10^3$. The results for $\mathrm{Re}=8\times10^3$ are presented as a series of close-up images in Fig. 2. In order to improve clarity for the quiver plots, the data was filtered to a much coarser grid.

These figures demonstrate the formation of stable Taylor vortices from vortex disturbances on the inner cylinder. This is in contrast to that observed for the laminar Taylor-Couette

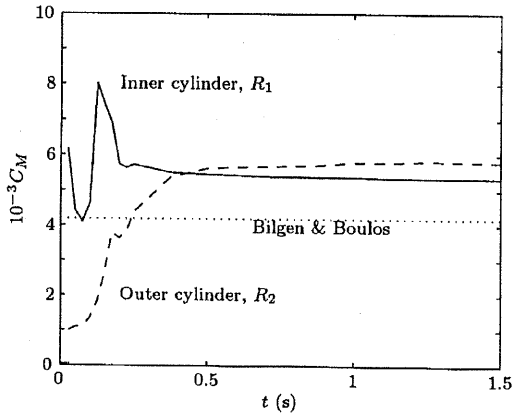

FIG. 3. Variation of the coefficient of friction with time, at $\mathrm{Re}=5\times10^3$.

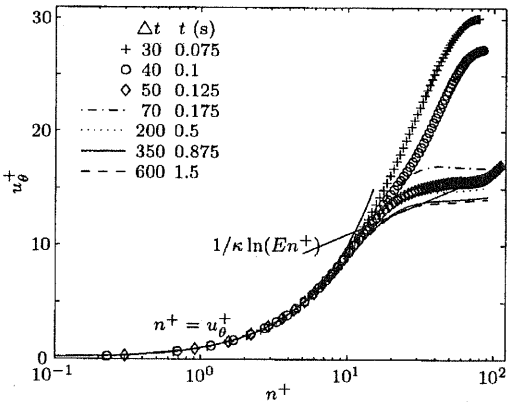

FIG. 4. Development of the mean azimuthal velocity profile, on the inner cylinder, at $\mathrm{Re}=5\times10^3$.

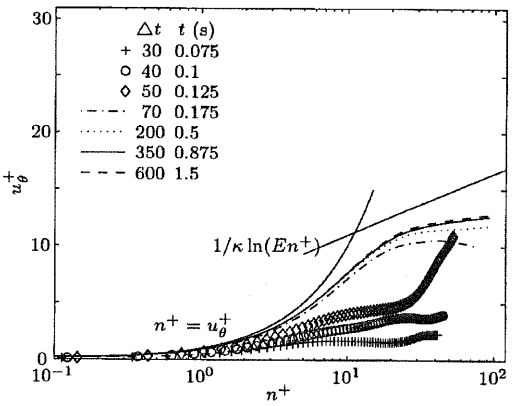

FIG. 5. Development of the mean azimuthal velocity profile, on the outer cylinder, at $\mathrm{Re}=5\times10^3$.

flow at Ta_c, where the Taylor vortices form at the wall ends. For $\mathrm{Re}=5\times10^3$, the following series of steps have been identified:

(1) Formation of pairs of ring-shaped vortices ($35\Delta t \rightarrow 50\Delta t$);
(2) mixing of ring-shaped vortices ($50\Delta t \rightarrow 75\Delta t$);
(3) mixing of both ring-shaped and Taylor vortices ($75\Delta t \rightarrow 100\Delta t$);
(4) stabilization of Taylor vortices ($100\Delta t \rightarrow$).

Initially a series of ring-shaped vortex pairs form at the inner cylinder as is clearly demonstrated in the first quiver plot in Fig. 2. Then, a phase of ring-shaped vortex mixing occurs due to the initial vortices spreading across the gap with new vortices forming at the inner cylinder, as seen, for example, at $36\Delta t$ in Fig. 2. During the third phase, Taylor vortices begin to form; but, as the flow has not fully developed, ring-shaped vortices are still being produced from just above the surface of the inner cylinder. Finally, when the flow is fully developed the Taylor vortices stabilize with no further vortices forming.

An initial pair of vortices is present at the block boundary at $35\Delta t$ in Fig. 1. This is due to the source of perturbation at the block interface being the most dominant. Two "dummy" cells were used to pass information between adjacent blocks, and hence to eliminate this source of perturbation more cells than the order of the discretization scheme are required. A premature perturbation such as this could also form in an experimental facility due to a large scratch on the surface of the inner cylinder.

The variation of skin friction

$$C_M = \frac{2M}{\pi\rho U_1^2 R_1^2 L} \tag{5}$$

with time t is presented in Fig. 3 and compared with the empirical equations of Bilgen and Boulos [16], where M denotes the moment on the inner cylinder and L is the axial length of the cylinders. The development of the azimuthal velocity profile

$$u_\theta^+ = u_\theta / \sqrt{\tau_w/\rho} \tag{6}$$

on the inner and outer cylinders with time is presented in Fig. 4 and 5, respectively, and compared with von Kármán's law of the wall,

$$u_\theta^+ = 1/\kappa \ln(En^+), \tag{7}$$

where $\kappa=0.419$ and $E=9.79$ [17].

These figures show an initial drop in skin friction at the wall as a laminar boundary layer begins to develop. This is illustrated for $30\Delta t$ as the mean azimuthal velocity profile is linear from the outer wall since no vortices have formed. At $40\Delta t$, the initial vortices have just started to form and the skin friction at the inner cylinder rises after the initial minimum in Fig. 3, and the velocity profile begins to tend away from the linear laminar profile towards that of a turbulent log law profile.

At $50\Delta t$, a peak in the skin friction is reached and the velocity profile tends towards the logarithmic profile. At this stage the initial vortices start to mix and the skin friction on the inner cylinder begins to decrease as the velocity profile across the gap grows. This is highlighted in Fig. 5 with the large increase in the mean azimuthal velocity profile from the outer cylinder for $50\Delta t \rightarrow 70\Delta t$. This corresponds to the sharp increase in skin friction at the outer cylinder in Fig. 3. The small secondary inflection in the growth of the skin friction, occurs at $\approx 100\Delta t$ due to the stabilization of the Taylor vortices. For $t > 200\Delta t$, the skin friction tends towards a constant value, along with the mean azimuthal velocity profile, on both the inner and outer cylinders.

IV. CONCLUSIONS

The simulations presented demonstrate the evolution from initial pairs of ring-shaped vortices on the inner cylinder to stabilized Taylor vortices. This occurs in four stages: formation of vortex pairs at the inner cylinder; mixing of ring-shaped vortices; a mixing phase of both the Taylor and ring-shaped vortices; stabilization of the Taylor vortices with no other vortices forming. This is distinctly different from the

formation of laminar Taylor vortices. Upon the initial formation of the ring-shaped vortices, there is a large peak in the shear stress on the inner cylinder and then the shear stress decays to around 20% above Bilgen and Boulos [16] results. After this peak the boundary layer profile tends towards von Kármán's law of the wall.

Despite the solutions being two dimensional, these provide a valuable insight into the flow physics at a fraction of the computational cost of three-dimensional simulations. However, simulations will need to be carried out in 3D to more accurately resolve the mixing within Taylor vortices and to solve the "herring-bone" conundrum associated with the possible existence of smaller vortices within stable Taylor vortices.

[1] A. W. Hughes, S. M. Abu-Sharkh, and S. R. Turnock, in *The Tenth International Offshore and Polar Engineering Conference* (ISOPE, Seattle, 2000).
[2] A. W. Hughes, Ph.D. thesis, School of Engineering Sciences, University of Southampton, 2000 (unpublished).
[3] D. P. Lathrop, J. Fineberg, and H. L. Swinney, Phys. Rev. A **46**, 6390 (1992).
[4] W. M. J. Batten, Ph.D. thesis, School of Engineering Sciences, University of Southampton, 2002 (unpublished).
[5] H. Görtler, NACA **TM-1371**940 (unpublished).
[6] A. Barcilon, J. Brindley, M. Lessen, and F. Mobbs, J. Fluid Mech. **94**, 453 (1979).
[7] A. Barcilon and Brindley, J. Fluid Mech. **143**, 429 (1984).
[8] T. Wei, E. M. Kline, S. H. K. Lee, and S. Woodruff, J. Fluid Mech. **243**, 47 (1992).
[9] G. I. Taylor, Proc. R. Soc. London, Ser. A **233**, 289 (1923).
[10] D. Coles, J. Fluid Mech. **75**, 1 (1976).
[11] E. L. Koschmieder, *Bénard Cells and Taylor Vortices*, 1st ed. (Cambridge University Press, Cambridge, 1993).
[12] Y. Takeda, J. Fluid Mech. **389**, 81 (1999).
[13] W. M. J. Batten, N. W. Bressloff, and S. R. Turnock, Int. J. Numer. Methods Fluids **38**, 207 (2002).
[14] J. E. Burkhalter and E. L. Koschmieder, Phys. Fluids **17**, 1929 (1974).
[15] N. W. Bressloff, Int. J. Numer. Methods Fluids **36**, 497 (2001).
[16] E. Bilgen and E. Boulos, Trans. ASME **95**, 122 (1973).
[17] S. B. Pope, *Turbulent Flows*, 1st ed. (Cambridge University Press, Cambridge, 2000).